Available online at www.sciencedirect.com
SCIENCE DIRECT®
Remote Sensing of Environment 84 (2003) 516–525
Remote Sensing of Environment
www.elsevier.com/locate/rse

Multi-angular optical remote sensing for assessing vegetation structure and carbon absorption

Jing M. Chen[a,*], Jane Liu[b], Sylvain G. Leblanc[b], Roselyne Lacaze[c], Jean-Louis Roujean[c]

[a] Department of Geography and Program in Planning, University of Toronto, 100 St. George St., Room 5047, Toronto, Ontario, Canada M5S 3G3
[b] Canada Centre for Remote Sensing, 588 Booth St., 4th Floor, Ottawa, Ontario, Canada K1A 0Y7
[c] GAME/CNRM (Météo France/CNRS), 42, avenue Gaspard Coriolis, 31057 Toulouse Cedex, France

Received 23 January 2002; received in revised form 16 September 2002; accepted 21 September 2002

Abstract

The utility of multi-angle optical remote sensing for terrestrial carbon cycle estimation is demonstrated through theoretical development, POLDER data analysis, and a case study of carbon cycle in a boreal forest. Progress in canopy-level photosynthesis modeling suggests that simpler big-leaf photosynthesis models are giving ways to more complex sunlit/shaded leaf separation models. This advancement in ecological modeling has increased the demand for advanced description of canopy architecture. Such demand may be mostly met through the use of multi-angle remote sensing techniques. In addition to leaf area index (LAI), another canopy parameter, the foliage clumping index, can be derived from multi-angle remote sensing. These two parameters are the basis for separating sunlit and shaded leaves. As leaf photosynthesis is nonlinearly related to incident radiation, such separation avoids the problems of big-leaf models that only make use of the total radiation absorption by the canopy without considering the distribution of radiation among leaves. A practical conclusion is that the traditional way of mapping the net primary productivity (NPP) through its correlation with the remotely sensed fraction of photosynthetically active radiation (FPAR) absorbed by plant canopies is only a very crude approximation and could be replaced with mapping LAI and clumping index and modeling NPP with advanced photosynthesis models. This is a step forward in remote sensing applications because single-angle remote sensing can only acquire information on the effective LAI related to the canopy gap fraction in the viewing direction and the amount of shaded leaf area is unknown.

Keywords: Multi-angular optical remote sensing; Vegetation structure; Carbon absorption

1. Introduction

Satellite remote sensing has been shown to be powerful tools for local (Band et al., 1991; Running et al., 1989), regional (Cihlar, Chen, & Li, 1997; Liu, Chen, Cihlar, & Chen, 2002; Veroustraete & Myneni, 1996), and global ecological applications (Hunt et al., 1996; Potter et al., 1993; Sellers et al., 1996). Previously, Landsat and SPOT images were often used for local applications, and only AVHRR images were available for regional and global applications. With the successful launches of new sensors, including VEGETATION on board SPOT-4 platform, MODIS, MISR and ASTER of the Terra mission, and the short-lived POLDER as part of ADEOS, our ability in ecological monitoring and modeling has been greatly improved. In addition, several forthcoming high spectral resolution and hyperspectral sensors as well as POLDER II sensor will soon be available. Technical improvements have been made in all remote sensing domains including spectral, angular, spatial and temporal resolutions. We are therefore presented with an unprecedented challenge to fully utilize these data to retrieve new information and achieve new knowledge.

As monitoring and modeling terrestrial carbon cycle has been one of the main drivers for many of the space missions, we will explore the utility of multiple angle remote sensing for terrestrial applications. Traditional remote sensing applications have mostly focused on extracting biophysical and biogeochemical information from multi-spectral signatures, and there were few demonstrations of the useful additional information retrieved from multi-angle data (e.g., Liang et

* Corresponding author. Tel.: +1-416-978-7085; fax: +1-416-946-3886.
E-mail address: chenj@geog.utoronto.ca (J.M. Chen).

0034-4257/02/$ - see front matter © 2002 Elsevier Science Inc. All rights reserved.
PII: S0034-4257(02)00150-5

al., 2000), until recently when airborne (Bréon et al., 1997) and space-borne (Bicheron & Leroy, 1999; Bréon & Colzy, 1999) multi-angle data became available. It is widely perceived that multi-angle measurements would be sensitive to vegetation structures and therefore can provide advanced structural descriptions. Recently useful angular signatures related to vegetation structure were found (Chen, Liu, Leblanc, Roujean, & Lacaze, 2001; Lacaze, Chen, Roujean, & Leblanc, 2002). The purpose of this paper is to demonstrate the implications of these findings on mapping the net primary productivity (NPP), which forms an important component of terrestrial carbon cycle.

2. Existing theories for NPP estimation

2.1. Empirical methods of mapping NPP

Solar radiation is the most critical driver of plant growth, as it provides the photosynthetically active radiation (PAR) for leaf photosynthesis and the thermal energy for biological activities. As the first approximation, the net amount of plant growth, in terms of net storage of carbon in plant tissues per unit ground surface area and time, i.e., NPP, is proportional to the total amount of radiation absorbed by the plant canopy (Monteith, 1972). As optical remote sensing provides measurements of the amount of reflected solar radiance from vegetated surfaces, it offers a means to obtain the total absorbed PAR (APAR) by plant canopies (Li & Moreau, 1996). NPP or Gross Primary Productivity (GPP) has therefore been mapped at the global scale (Goetz & Prince, 1998; Potter et al., 1993; Prince & Goward, 1995) through its linear relationship with APAR, i.e.,

$$\mathrm{NPP} = \varepsilon \mathrm{APAR} \quad (1)$$

where ε is the conversion rate of APAR into NPP. APAR is calculated as PAR × FPAR, where PAR is the incoming PAR and FPAR is the fraction of PAR absorbed by a vegetation canopy. As FPAR can be derived using remote sensing data, Eq. (1) is useful for regional and global applications. Since ε is species dependent, a concurrent land cover map is often used to implement this method. There has been increasing recognition of the importance of autotrophic respiration that is not directly related to APAR but is related to biomass and temperature, and therefore, Eq. (1) has been reformulated in various ways (Prince & Goward, 1995; Ruimy, Dedieu, & Saugier, 1996).

2.2. Simple process models for mapping NPP

Farquhar's leaf-level photosynthesis model (Farquhar, von Caemmerer, & Berry, 1980) has been widely used to simulate the canopy-level photosynthesis with various methods for scaling from leaf to canopy. The model allows simulations of photosynthetic processes under various weather conditions and therefore is a methodological improvement over the empirical methods mentioned above. Big-leaf models are the simplest of this kind and have been used for regional (Kimball, Thornton, White, & Running, 1997) and global (Hunt et al., 1996; Sellers, Berry, Collatz, Field, & Hall, 1992) NPP calculations. These models are driven by remote sensing inputs of land cover types or leaf area index (LAI) or both. The LAI, in this case, is used to calculate the APAR and hence the mean PAR irradiance on leaves to drive the Farqhuar leaf-level model for canopy-level photosynthesis calculations. An improvement is made to such an approach by considering the vertical gradient of PAR irradiance on leaves (Sellers et al., 1992). Although the mathematical description of the effect of APAR on photosynthesis in big-leaf models is different from that of Eq. (1), the essential contribution of remote sensing to NPP mapping is very similar between these two methods.

3. Recent advances in canopy photosynthesis modeling and new data demand

Although aforementioned methods are effective, they represent only the crude first approximations of the complicated photosynthetic processes in plant canopies with various foliage architectures. As we are now afforded with many new remote sensing capabilities, alternatives are to be sought.

Big-leaf models for canopy evapotranspiration (ET) estimation have a long history starting from the Penman–Monteith equation (Monteith, 1973). Big-leaf ET models have been considered to be adequate for simulating water fluxes measured above plant canopies (McNaughton & Jarvis, 1991; Raupack & Finnigan, 1988) in spite of questions regarding within-canopy anti-gradient flows in the 1980s (see review by Shuttleworth, 1989). However, few tests of big-leaf photosynthesis models were made until recently when simultaneous CO_2 flux measurements above and below plant canopies (Black et al., 1996; Goulden et al., 1997) were available for such model tests (Chen, Liu, Cihlar, & Goulden, 1999). Chen et al. (1999) found that while the Penman–Monteith ET model simulated measured H_2O fluxes well, big-leaf photosynthesis models suffered several major drawbacks and compared poorly with measurements at hourly and daily time steps. Although big-leaf models can be calibrated to specific sites for estimating seasonal trends of photosynthesis, the calibrated coefficients used in the models would be site specific. They concluded that big-leaf photosynthesis models are not suitable for remote sensing applications as it lacks generality required for large area applications. Lai, Katul, Oren, Ellsworth, and Shafer (2000) also found the inadequacy of a big-leaf photosynthesis model for stand-level simulations. Chen et al. (1999) successfully tested an alternative using the sunlit/shaded leaf separation strategy

based on Norman (1993). Independent works of Du Pury and Farquhar (1997) and Wang and Leuning (1998) also came to the same conclusion in favor of sunlit/shaded leaf models for simulating canopy-level photosynthesis. The other alternative based on multilayer strategy (Bonan, 1995; Foley, 1994) seems to receive less attention in recent years as models of this type are not as effective in capturing the radiation gradient within the canopy as the sunlit/shaded leaf models. Nevertheless, multilayer models have the irreplaceable advantage of describing the different biological properties of leaves in different layers, such as nitrogen content and photosynthetic capacity, as time-integrated outcomes of the light gradient with the depth into the canopy (Sellers et al., 1992).

Since it has been demonstrated that sunlit/shaded-leaf and multilayer models, or combination of them, are more reliable than big-leaf models, we then need to know how these models can be implemented using remote sensing inputs. LAI is the basic canopy structural parameter needed for any process-based canopy photosynthesis models. Regional (Chen et al., 2002; Liu, Chen, Cihlar, & Chen, 1999) and global (Myneni, Nemani, & Running, 1997; Sellers et al., 1996) LAI maps have been derived from AVHRR images. However, the single LAI parameter is insufficient to describe the effect of canopy architecture on radiation absorption and distribution in the canopy. Vegetation at the Earth's surface has various levels of foliage organization. Herbaceous canopies (crops and grasses) generally have simple structures with leaves more or less randomly distributed in space, whereas foliage in forests is often organized in structures at various hierarchical levels, such as shoots, branches, whorls, tree crowns, and tree groups. We therefore need at least one additional parameter to characterize the leaf spatial distribution pattern. The foliage clumping index (Chen, 1996a; Nilson, 1971) has been shown to be a good choice for this purpose. The use of a clumping index is critical in any photosynthesis models, either empirical through the calculation of APAR or process-based through the calculation of the average PAR irradiance on all leaves or on sunlit and shaded leaves separately. However, the clumping index is a particularly important input in sunlit/shaded leaf models (Chen et al., 1999) as its value greatly modifies the amounts of sunlit and shaded leaves. As foliage clumping increases at a given LAI, i.e., leaves are more aggregated in clumps, the amount of sunlit leaves decreases and that of shaded leaves increases, changing the final outcome of canopy photosynthesis. The use of the clumping index therefore captures the ecological importance of existing canopy architectural difference of various vegetation types. In mapping NPP of boreal ecosystems (Liu et al., 1999), one value of clumping index was assigned to each cover type. However, as the clumping index can vary considerably for a cover type, it is highly desirable to map the spatial distribution of this index using remote sensing data.

4. Deriving canopy architectural information from multiple angle remote sensing

The essential information for leaf area contained in optical remote sensing measurements made at a few angles is the effective LAI, taken as the product of LAI and the clumping index (Chen, 1996a). This principle was demonstrated using Landsat-5 data for boreal conifer forests (Chen & Cihlar, 1996). This is because radiative signals from shaded leaves are weak and the total reflected solar radiance measured at a few angles results mostly from sunlit leaves (Hall, Huemmrich, Goetz, Sellers, & Nickeson, 1992). However, if similar measurements are made over a wide range of view zenith angles, the pattern of variation in the amount of sunlit leaves seen at the various angles contains the information of shaded leaves. To demonstrate the physical principles of deriving shaded leaf information from multiple angle remote sensing, some typical bidirectional reflectance distribution functions (BRDF) are shown in Fig. 1. The points in Fig. 1 are measurements made in June 1998 by the POLDER-I sensor onboard of ADEOS (Bréon et al., 1999) from three uniform pixels of grassland, deciduous forest and conifer forests in Canada. The curves are simulated using a kernel-based model (Leblanc et al., 2001) for BRDF on the principal solar plane formed by the sun, satellite and ground target, while the data points are all

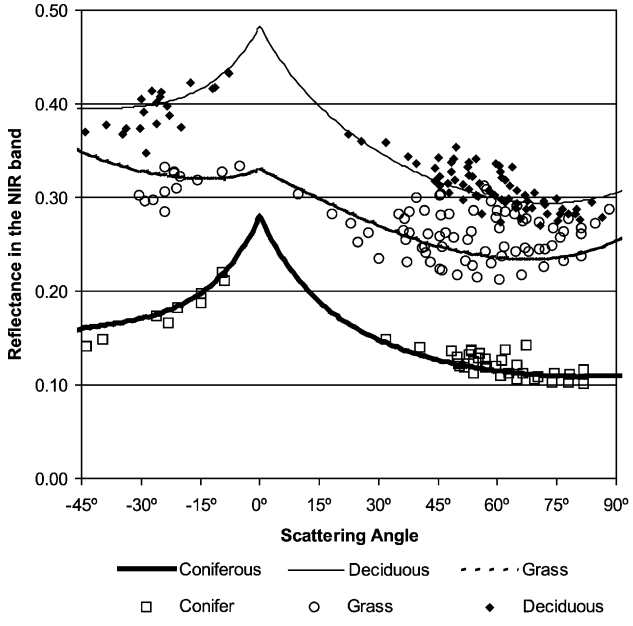

Fig. 1. Typical bidirectional reflectance distribution function (BRDF) curves for three surface types: grassland, deciduous and conifer forests. Points are ADEOS POLDER measurements at all angles in the hemisphere in June 1998 in Canada for a selected uniform pixel for each cover type. The curves are simulations using a model for the BRDF on the principal solar plane. The scattering angle is the difference between the sun angle and the view angle to the ground target. The center of the pixels are (111°15′41″ W, 50°58′43″ N) for grassland, (75°33′19″ W, 46°41′14″ N) for deciduous forest; and (75°07′18″ W, 48°51′51″ N) for conifer forests.

available measurements for a pixel at various observation angles in the hemisphere. The solar zenith angle at the various dates of measurements varied in a range from 24° to 31°. The data are shown against the scattering angle, which is the angle between the illumination (sun) and observation (satellite). Different illumination and view geometries in the measurements contribute to the scattering of data points, and the model only represents one plane in the hemisphere. The observed and modeled reflectances of all three cover types exhibit large variations against the scattering angle. The reflectances were the largest at the hotspot, i.e., the scattering angle is zero where the illumination and observation angles coincide, and the smallest at the darkspot where shadows created by the vegetation canopy is maximally observed. These cases are markedly different from the Lambertian case (not shown) that would be a horizontal line in the plot. A Lambertian surface makes isotropic reflection, meaning no variation of the reflected radiance with view angle. The measured and modeled BRDFs from the three types of vegetation covers are distinctly different in the overall magnitude of near-infrared reflectance and the variation pattern. Grassland is generally covered by leaves randomly distributed as a turbid medium. The grass canopy presents a variable amount of shadows to the sensor as the view angle changes. Conifer with its highly organized canopy architecture shows a BRDF curve with a relatively large amplitude. Deciduous forest is the intermediate case. The magnitude of the hotspot is determined by both optical properties of the foliage and background (soil, moss and understory) and canopy architecture determining the ability of the canopy to trap photons. The darkspot is also determined by the optical properties of foliage and background, but more dominantly by the amount of the shadow created by the canopy. The darkspot of the conifer pixel is much darker than that for grass and deciduous forest pixels because the large amount of shadows on the ground and on the shaded side of conifer tree crowns observed at the darkspot. The shaded tree crown component may be particularly important in this context as the tree crown is one of the most important scales of foliage clumping. In addition to tree crown size and tree number density, the foliage density in the tree crowns has a pronounced effect on the overall foliage clumping. The denser the crowns, the more clumped is the canopy, and the more shadows on the tree crowns will be observed in the forward scattering side. This is the basic physics of relating canopy-level foliage clumping to the amplitude of BRDF curves. Quantitatively, the clumping index can be related to an angular index formulated using the hotspot and the darkspot values of the BRDF curve. It is named as the Hotspot–DarkSpot index (HDS), and is mathematically expressed as (Chen et al., 2001; Lacaze et al., 2002)

$$\mathrm{HDS} = \frac{\rho_{\mathrm{HS}} - \rho_{\mathrm{DS}}}{\rho_{\mathrm{DS}}} \tag{2}$$

where ρ_{HS} is the reflectance at the hotspot, and ρ_{DS} is the reflectance at the darkspot. The value of the darkspot is not only determined by the canopy geometry but also leaf optical properties controlling the amount of multiple scattering in the canopy. Hence, the difference in the reflectance at hotspot and darkspot is normalized against that at the darkspot to reduce the influence of leaf optical properties on the index and to accentuate the importance of canopy geometry. The values of HDS for the three cases shown in Fig. 1 are 0.38 for grassland, 0.66 for deciduous forest, and 1.43 for conifer forest.

Using the space-borne POLDER data acquired in late May and June 1998 over Canada and available ground data of foliage clumping index (Ω) acquired by TRAC (Chen, Rich, Gower, Norman, & Plummer, 1997), the relationship between HDS and Ω was investigated. Fig. 2 shows a summary of the investigation, where HDS for each of the three major cover types is taken as the average of all 7 × 7-km pixels dominated by one of cover types, and Ω is taken as the mean value of available TRAC measurements. As hotspot and darkspot are not routinely sampled by POLDER, models were used to fit BRDF curves to the available POLDER data points and to find the hotspot and darkspot values (Lacaze et al., 2002; Leblanc et al., 2001). Based on the available POLDER data and limited ground data for Ω, the relationship between HDS and Ω as shown in Fig. 2 appears to be approximately linear, i.e.,

$$\Omega = a + b\mathrm{HDS} \tag{3}$$

where a and b are coefficients determined by the linear regression. These coefficients found from the regressions are somewhat different between red and near-infrared (NIR) bands, suggesting that the influence of leaf optical properties is not totally eliminated by HDS. However, these empirical relationships give us confidence in retrieving canopy structural information from multi-angle remote sensing. These relationships have been refined using airborne POLDER data over boreal forests in Canada (Lacaze et al., 2002). Sandmeier and Deering (1999) also found improvements in boreal land cover classification using an angular index. Through model inversion, it has also been shown that multiple angle measurements improve LAI retrieval results over those using only single-angle measurements (Diner et al., 1999; Knyazikhin et al., 1998).

The five-scale model (Leblanc & Chen, 2001) with a new multiple scattering scheme (Chen & Leblanc, 2001) was used to explore the generality and reliability of the empirical relationships shown in Fig. 2 and to investigate whether better angular indices can be devised. The five-scale simulations were made with several input structural parameters varying in wide ranges including stem density (500–3500 stems/ha), crown height (1–20 m), crown radius (0.5–3 m), and LAI (0.5–8). The foliage density inside tree crowns resulting from this parameter setting ranges from 0.05 to 30 m^2/m^3. The simulated results are summarized in Fig. 3. As shown in Fig. 3 a reasonably

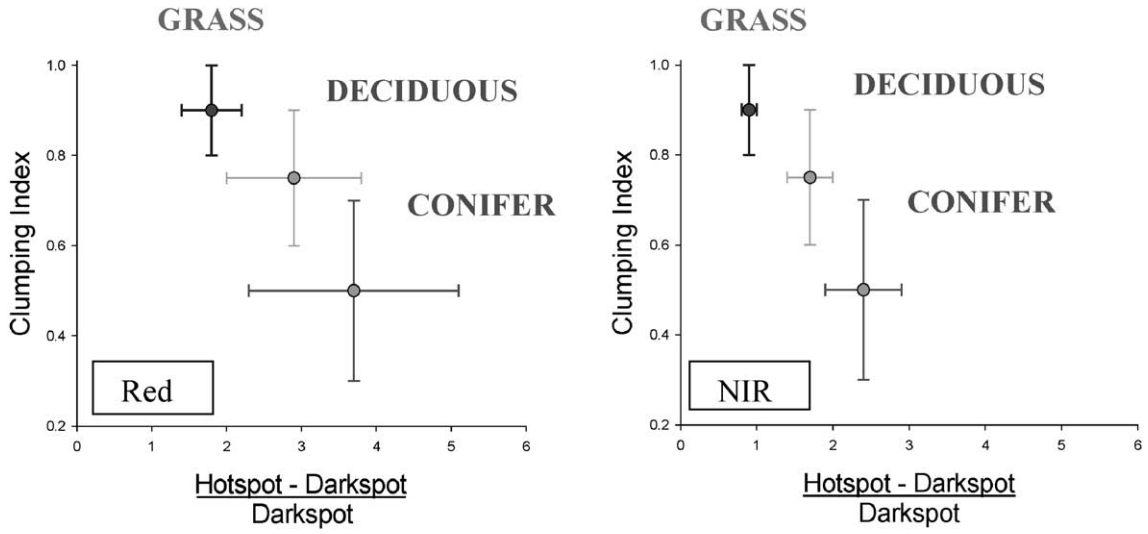

Fig. 2. The relationship between the Hotspot–Darkspot angular index (HDS) and the clumping index (Ω) found from space-borne POLDER data over three land cover types in Canada (after Chen et al., 2001; Lacaze et al., 2002). The ranges of Ω are from all available ground measurements made in Canada, and the ranges of HDS are standard deviations of all uniform 7-km pixels (with >50% dominant cover type) in Canada.

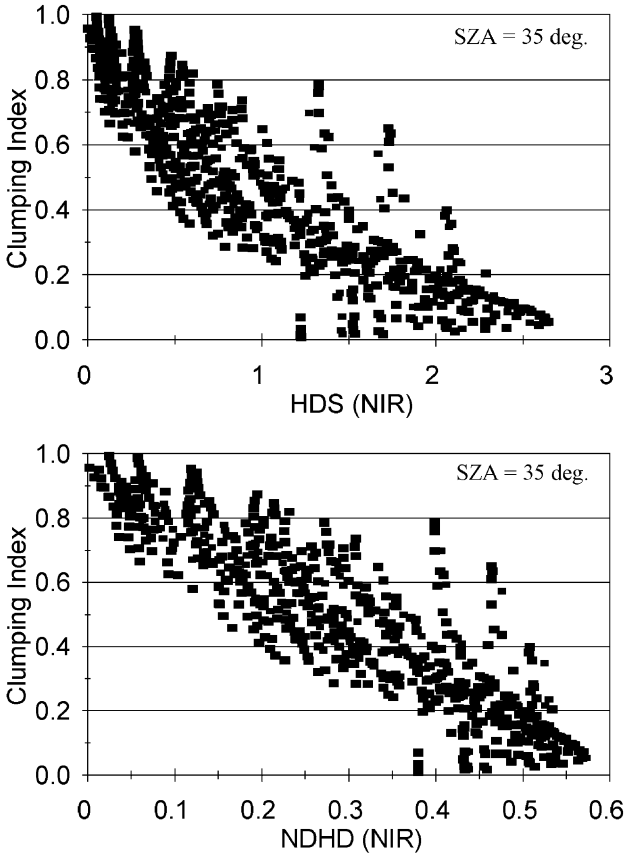

Fig. 3. Relationships between clumping index and angular indices NDHD and HDS simulated using the five-scale model for black spruce forest stands at the solar zenith angle (SZA) of 35°. The clumping index depends on canopy architectural parameters such as stem density, crown size, foliage density within tree crowns, and tree spatial distribution, and shoot level clumping. The NDHD and HDS are obtained from the simulated bidirectional reflectance distribution function on the principal solar plane.

strong relationship between Ω and HDS exist for a wide range of canopy conditions until extreme of sparseness or denseness of the canopy is reached (Leblanc et al., 2001). However, the general relationship between Ω and HDS appears to be nonlinear when all modeled results including extreme canopy conditions are used. We therefore also tested another angular index (Leblanc et al., 2001), named the Normalized Difference between Hotspot and Darkspot (NDHD), defined as NDHD=$(\rho_{HS}-\rho_{DS})/(\rho_{HS}+\rho_{DS})$. The general relationship between Ω and NDHD as simulated is linear, suggesting NDHD may be a better index than HDS. However, more comprehensive investigation is needed before solid conclusions on the choice of angular indices are drawn.

5. Importance of foliage clumping in canopy radiation and photosynthesis modeling

5.1. Radiation modeling

The importance of clumping index in canopy radiation modeling may be demonstrated using the following equation for calculating the radiation penetration through a plant canopy (Nilson, 1971):

$$P(\theta) = e^{-G(\theta)L\Omega/\cos\theta} \quad (4)$$

where $P(\theta)$ is the probability of light penetration through the canopy at zenith angle θ; L is the LAI; and $G(\theta)$ is the mean projection of leaf normals in the direction of θ. $G(\theta)$ is determined by the leaf angle distribution, while the clumping index Ω characterizes the spatial distribution of leaves. The importance of Ω in radiation modeling is two folds: it affects both FPAR and the radiation distribution in the

canopy. Mathematically, FPAR can be calculated as (Chen, 1996b; Goward & Huemmrich, 1992)

$$\mathrm{FPAR} = 1 - \rho_{\mathrm{PARabove}} - (1 - \rho_{\mathrm{PARbelow}})P(\theta) \quad (5)$$

where ρ_{PARabove} and ρ_{PARbelow} are the PAR albedos above and below the canopy, respectively. Using ρ_{PARabove}, the fraction of PAR directly reflected off the top of the canopy is considered, and using ρ_{PARbelow}, the small portion of PAR absorbed by the canopy after reflection by the surface underneath the canopy is also included.

FPAR is often estimated based on Eqs. (4) and (5) with an input of LAI without considering the clumping, i.e., Ω is assumed to be unity. If the input LAI is obtained indirectly using optical instruments, such as LAI-2000, it is actually the effective LAI denoted by L_e, meaning that it is the product of LAI and Ω, i.e., $L_e = \Omega L$ (Chen, 1996a). For this case, the calculation of FPAR is accurate. Reasonably accurate LAI values can be obtained using allometric equations established from destructive sampling (Gower et al., 1977). When the LAI obtained in this way is used without considering the clumping effect, FPAR calculations will be positively biased. For example, a typical boreal conifer forest has LAI of 4 and Ω of 0.5. Taking the usual value of 0.5 for $G(\theta)$ under the assumption of random leaf angle distribution, the probability of radiation penetration through the canopy at $\theta = 45°$ will be 0.06 without considering clumping (i.e., $L = 4$ and $\Omega = 1.0$, the random case), but it will be 0.24 when the clumping is considered (i.e., $L = 4$ and $\Omega = 0.5$). If albedos above and below the canopy are taken as 5% and 6%, respectively (Chen, 1996b), FPAR of the canopy will be 0.894 in the random case but 0.724 in the clumped case. For such a case, the relative error in FPAR estimation without considering the clumping effect will be 23.5%, i.e., (0.894−0.724)/0.724. Such a magnitude of error cannot be ignored for many applications.

The effect of clumping on radiation distributions within plant canopies is the main issue that multi-angle remote sensing can make a critical contribution. For the above case, one may argue that since only an accurate effective LAI is needed for FPAR calculations and it can be accurately measured using optical instruments, we do not need to bother with canopy structure and the actual LAI. However, at a given value of effective LAI, the ratio of shaded to sunlit leaves will be very different whether or not the foliage is clumped, even though FPAR remains the same. The equations used for the sunlit and shaded LAI calculations are based on Norman (1993), and modified to consider the clumping effect (Chen et al., 1999), i.e.:

$$L_{\mathrm{sun}} = \frac{\cos(\theta)}{G(\theta)}\left[1 - \exp\left(-G(\theta)\Omega L/\cos(\theta)\right)\right] \quad (6)$$

$$L_{\mathrm{shaded}} = L - L_{\mathrm{sun}} \quad (7)$$

The effects of canopy geometry on the separation of sunlit and shaded leaves are described through the parameter $G(\theta)$ for the foliage angular distribution pattern and Ω for the spatial distribution pattern. Parameters such as tree crown size, density, and shape influence the value and angular variation pattern of Ω (Kucharik, Norman, Murdock, & Gower, 1997). Geometrical models can be used to investigate suitable forms of these two parameters for different applications.

Using the same example as the calculation of APAR above, i.e., $L = 4$, $\Omega = 0.5$, $G(\theta) = 0.5$, and $\theta = 45°$, the amount of sunlit LAI will be 1.07, and the shaded LAI will be 2.93. If the effective LAI, i.e., $L_e = 4 \times 0.5 = 2.0$, were taken as the actual LAI, the sunlit LAI and FPAR would be the same (if the small effect of multiple scattering within the canopy is ignored) but the shaded LAI would be reduced to 0.6. This problem of underestimating the shaded LAI may be a common problem facing LAI retrieval from optical measurements at nadir because optical signals at nadir mostly respond to the canopy gap fraction (or sunlit leaves) in the vertical direction. The inversion of the gap fraction using Eq. (4) provides only the effective LAI, not the true LAI. Fig. 4 shows systematically how the sunlit and shaded LAI varies with clumping index when L_e is taken as a constant of 2.0 and θ is fixed at 45°. Since L_e is constant, the sunlit LAI is invariant at the same sun angle as the clumping index changes, but the shaded LAI increases dramatically as the clumping index decreases (more clumped), so does the total LAI. It is intuitively understandable that the more clumped a canopy is, the more shaded leaves are beneath sunlit leaves. The fundamental question is then whether it matters to ignore the contributions of shaded leaves to photosynthesis and carbon absorption in plant canopies.

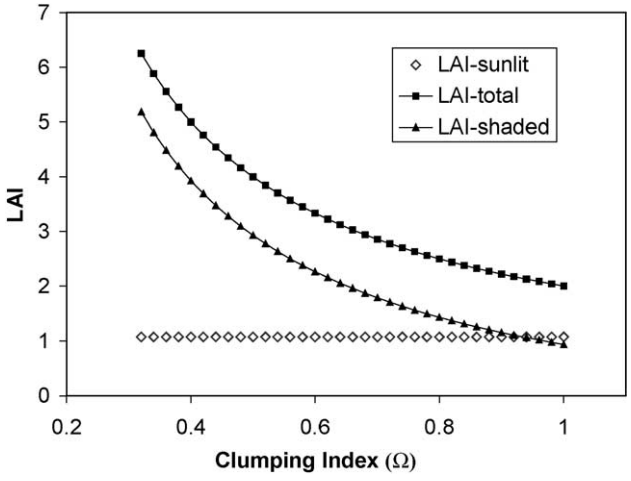

Fig. 4. Variation of sunlit and shaded leaf area index (LAI) with clumping index when the effective LAI (L_e) is taken as a constant of 2.0. Nadir-view optical multi-spectral remote sensing signals contain information on the effective LAI rather than the actual LAI. As the clumping index decreases (more clumped) at the same effective LAI, the shaded LAI and the total LAI increase. Note: $L_e = \mathrm{LAI}^*\Omega$.

5.2. Photosynthesis modeling

To understand the importance of shaded leaves in plant canopies, we investigated the contribution of shaded leaves to the total canopy photosynthesis as an example. For this purpose, we only investigate the cases with a constant effective LAI (L_e) as an input with varying clumping index (Ω), while the obvious effect of clumping on APAR (see Section 5.1) and photosynthesis at the same LAI is not included here. When L_e remains the same, the amount of sunlit leaves and APAR will not change with clumping, but the amount of shaded leaves will increase with an increasing degree of clumping. Although shaded leaves in the canopy receive much less radiation than the sunlit leaves, they can make a large contribution to the total canopy photosynthesis. This is because (i) the mean PAR irradiance on shaded leaves not only originates from the sky diffuse light but also from multiple scattering within the canopy and (ii) the response of leaf photosynthesis to the level of irradiance is not linear. Leaf photosynthesis generally becomes nearly saturated at a level only about 1/3 of the full sunlit (Fig. 5). This light response curve without including the dark respiration is calculated based on a common formulation (Bonan, 1995; Jarvis & Morison, 1981). Much of the solar energy reaching sunlit leaves is therefore not fully utilized for photosynthesis. It was found that the light use efficiency for diffuse light was several times larger than that of direct light for boreal forests (Gu et al., 2002). Indeed, shaded leaves can, under bright sky conditions, produce photosynthesis at a considerable magnitude compared with sunlit leaves. When the foliage is clumped, most leaves are in shade, even at the solar noon, and the collective contribution of shaded leaves may exceed the sunlit leaves on a daily basis. For a spherical leaf angle distribution, i.e., $G(\theta)=0.5$, the maximum sunlit LAI is 2, and if total LAI is larger than 4, most leaves are shaded in a given time.

The above arguments are demonstrated using the Boreal Ecosystem Productivity Simulator (BEPS) (Chen et al., 1999; Liu et al., 1999) which calculates the total canopy photosynthesis (A) as the sum of sunlit and shaded leaf contributions (Norman, 1993), i.e.,

$$A = A_{\text{sun}} \cdot L_{\text{sun}} + A_{\text{shade}} \cdot L_{\text{shade}} \quad (8)$$

where A_{sun} and A_{shade} are the photosynthesis rates for unit sunlit and shaded leaf areas, respectively. This type of models has been validated using experimental data (Chen et al., 1999; Kim & Verma, 1991). Chen et al. (1999) developed a set of equations for calculating the mean PAR irradiances on sunlit and shaded leaves based on a simple two-stream model. A is considered as the gross primary productivity (GPP), and NPP is calculated as the difference between GPP and the autotrophic respiration. The latter is a function of temperature and biomass, which is separated into leaves, stems and roots (Liu et al., 1999).

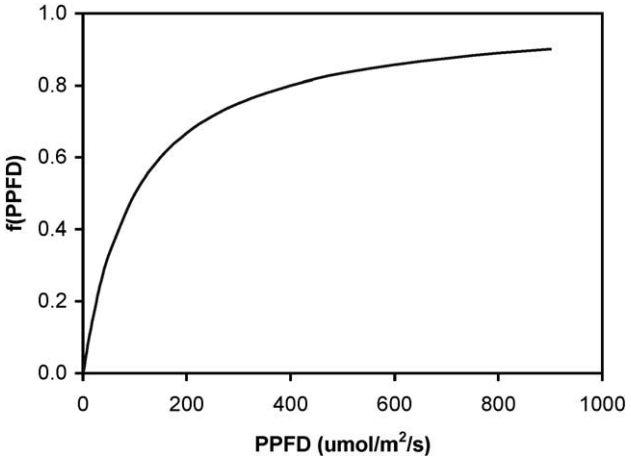

Fig. 5. A typical response curve of leaf photosynthesis to the photosynthetic photon flux density (PPFD) incident on the leaf surface.

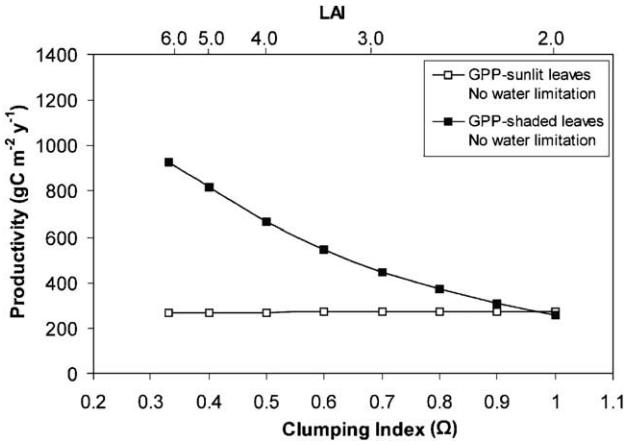

Fig. 6. Gross primary productivity (GPP) simulated for sunlit and shaded leaves separately, showing the importance of shaded leaves in their collective contribution to the total canopy photosynthesis. In all these simulations, the effective LAI (L_e) = 2.0, so APAR and the amount of sunlit leaves are unchanged, but the amount of shaded leaves increases with decreasing clumping index (more clumped). The results are simulated using BEPS (Liu et al., 1999) for a mature black spruce site in Canada. Note: $L_e = \text{LAI}*\Omega$.

BEPS was run with a dataset from an old black spruce site. The actual daily meteorological data (including air temperature and humidity, precipitation, total solar radiation) for the whole year of 1994 (Goulden et al., 1997; Wofsy et al., 2000) were used in the model simulation. The LAI and clumping index of the stand were measured with TRAC to be 4.0 and 0.5, respectively, resulting in $L_e = 2.0$ (Chen, 1996a). Holding L_e constant, i.e., LAI $\times\ \Omega = 2.0$, we simulated the effects of clumping on the photosynthesis (GPP) of sunlit and shaded leaves in this particular canopy (Fig. 6). To reveal the fundamental effects of foliage architecture on photosynthesis, we turned off the soil water balance module during these simulations, so that the leaf photosynthesis is not limited by the water availability under the local environmental conditions. Without water limitation, the total GPP of all sunlit leaves in the canopy remains about the same, while the total GPP of all shaded leaves

increases drastically as the clumping increases. The increases solely result from the increases in the shaded LAI as shown in Fig. 4, although the main PAR irradiance on shaded leaves decreases as clumping increases. As the sunlit and shaded leaf separation depends not only on canopy structure but also on solar zenith angle, the separation in daily calculations is not exactly the same as that shown in Fig. 4 calculated at a fixed angle of 45°, but they are similar. It is shown that in boreal forests, shaded leaves generally outdo sunlit leaves in their contribution to the total GPP of the canopy. The use of clumping index then becomes critical in canopy-level GPP assessment, given the fact that for the same L_e measured by optical remote sensing at one angle, the amount of shaded leaves can vary depending on the clumping index.

As the outcome of the results shown in Fig. 6, the responses of GPP and NPP to changes in the clumping index at the same L_e are summarized in Fig. 7. NPP is GPP less autotrophic respiration, which only changes slightly with changes in the amount of shaded leaves for this set of simulations. As the effective LAI remains unchanged in the simulations, the total LAI decreases as the clumping index increases. To be more realistic in Fig. 7, the BEPS simulations were done under two water regimes: no soil water limitation (as shown in Fig. 6) and with water limitation. In the water limitation case, the actual precipitation and daily weather data were used to calculate the soil water balance and determine the predawn soil and leaf water potentials and therefore the stomatal limiting factor (Jarvis & Morison, 1981). The modeled GPP and NPP values generally increase with increasing clumping (decreasing clumping index). These increasing trends are monotonic if water limitation is not considered, but reversals of the trends at low values of the clumping index are found under the water limitation regime. When soil water is not limiting, the additional

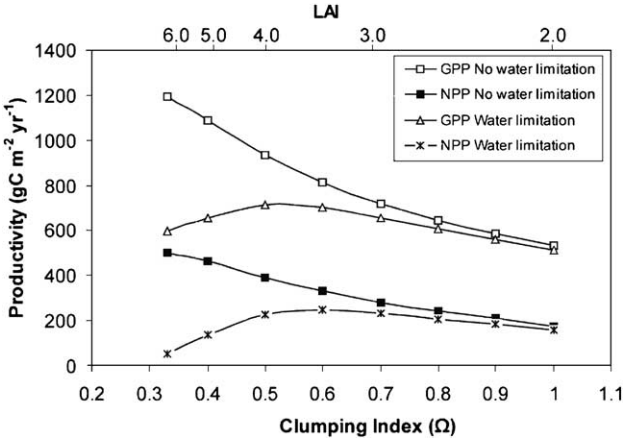

Fig. 7. Gross primary productivity (GPP) and net primary productivity (NPP) as affected by the clumping index for a constant value of the effective LAI (L_e = 2.0). The "no water limitation" case is the extension of the results shown in Fig. 6, while the "water limitation" case is calculated based on changes in leaf stomotal conductance with soil water moisture simulated using the actual data for the boreal forest. Note: L_e = LAI*Ω.

shaded leaves contribute more and more to the total canopy photosynthesis as the foliage becomes more clumped, but when water is limiting, the additional shaded leaves transpire more water and the water potential of soil decreases, resulting in a reduction in stomatal conductance, and hence GPP and NPP. Under the "no water limitation" case, both GPP and NPP decrease about 50% from the realistic clumped case (Ω = 0.5) to the hypothetical random case (Ω = 1), suggesting that the additional shaded leaves in the clumped scenario can double both GPP and NPP. When the water limitation is considered, the decrease in GPP from Ω = 0.5 to Ω = 1 is 37%, and the corresponding decrease in NPP is 23%. These large magnitudes of NPP variation with foliage clumping in both cases are alarming, showing the potential benefit of investments in space programs for multiple angle remote sensing.

It is also interesting to see in Fig. 7 that the modeled maximum GPP and NPP of the stand occur at a clumping index of about 0.5, corresponding to the actual measured value. This suggests that foliage clumping exists with some ecological significance. It is possible that conifer species adapt to the boreal environment through maximizing the diffuse light use efficiency, but there is a limit to the amount of shaded leaves that a canopy can support because of the limitation of soil water availability in the summer months, which can sometimes be very dry. The canopy architecture of boreal conifer stands consisting of long and narrow tree crowns of dense foliage may therefore evolve from the needs to minimize snow damages in the winter and to maximize the light use efficiency in the summer. If only the total radiation absorption was considered, we would have ignored the ecological importance of the canopy architecture containing large proportions of shaded leaves.

6. Implications on the use of multi-angle remote sensing data

For ecological applications of optical remote sensing, two parameters describing the status of vegetation canopy are often used alternately. One is LAI, and the other is the fraction of photosynthetically active radiation (FPAR) absorbed by the canopy. From the cases demonstrated in Figs. 6 and 7, it can be inferred that these two parameters actually represent two different approaches in ecological modeling. If NPP is calculated from APAR using FPAR without considering how APAR is shared among the sunlit and shaded leaves, the NPP estimation is only the crude first approximation. However, if LAI is used merely to calculate APAR, no much additional progress is made. With multi-angle optical remote sensing, we are now able to derive not only the correct LAI but also the clumping index. For this case, the canopy-level photosynthesis is not calculated from APAR but from the PAR irradiance on sunlit and shaded leaves separately, and the results are expected to be more accurate than the approach based on FPAR. We therefore

suggest that we should abandon the use of FPAR and employ LAI and clumping index when multiple angle remote sensing data are available.

7. Conclusion

Multiple angle remote sensing techniques are so far underutilized for ecological applications. With the availability of multi-angle remote sensing data, the traditional way of mapping NPP through mapping FPAR may be replaced with modeling NPP using canopy architectural parameters derived from multi-angle remote sensing. LAI and clumping index are two equally important canopy structural parameters for plant growth and terrestrial carbon cycle modeling.

Acknowledgements

The senior author thanks the Natural Science and Engineering Research Council (NSERC) of Canada for the financial support to this work. We are indebted to Dr. Josef Cihlar of Canada Centre for Remote Sensing for useful discussions.

References

Band, L. E., Peterson, D. L., Running, S. W., Dungan, J., Lathrop, R., Coughlan, J., Lammers, R., & Pierce, L. L. (1991). Forest ecosystem processes at the watershed scale: basis for distributed simulation. *Ecological Modelling*, *56*, 171–196.

Bicheron, P., & Leroy, M. (1999). A method of biophysical parameter retrieval at global scale by inversion of a vegetation reflectance model. *Remote Sensing of Environment*, *67*, 251–266.

Black, T. A., den Hartog, G., Neumann, H. H., Blanken, P. D., Yang, P. C., Russell, C., Nesic, Z., Lee, X., Chen, S. G., Staebler, R., & Novak, M. D. (1996). Annual cycle of water vapour and carbon dioxide fluxes in and above a boreal aspen forest. *Global Change Biology*, *2*, 101–111.

Bonan, G. B. (1995). Land–atmosphere CO_2 exchange simulated by a land surface process model coupled to an atmospheric general circulation model. *Journal of Geophysical Research*, *100*, 2817–2831.

Bréon, F. M., & Colzy, S. (1999). Cloud detection from the spaceborne POLDER instrument and validation against surface synoptic observations. *Journal of Applied Meteorology*, *38*(6), 777–785.

Bréon, F. M., Vanderbilt, V., Leroy, M., Bicheron, P., Walthall, C. L., & Kalshoven, J. E. (1997). Evidence of hot spot directional signature from airborne POLDER measurements. *IEEE Transactions on Geoscience and Remote Sensing*, *35*, 479–484.

Chen, J. M. (1996a). Optically-based methods for measuring seasonal variation of leaf area index in boreal conifer stands. *Agricultural and Forest Meteorology*, *80*, 135–163.

Chen, J. M. (1996b). Canopy architecture and remote sensing of the fraction of photosynthetically active radiation in boreal conifer stands. *IEEE Transactions on Geoscience and Remote Sensing*, *34*, 1353–1368.

Chen, J. M., & Cihlar, J. (1996). Retrieving leaf area index for boreal conifer forests using Landsat TM images. *Remote Sensing of Environment*, *55*, 153–162.

Chen, J. M., & Leblanc, S. G. (2001, May). Multiple-scattering scheme useful for hyperspectral geometrical optical modelling. *IEEE Transactions on Geoscience and Remote Sensing*, *39*(5), 1061–1071.

Chen, J. M., Liu, J., Cihlar, J., & Goulden, M. L. (1999). Daily canopy photosynthesis model through temporal and spatial scaling for remote sensing applications. *Ecological Modelling*, *124*, 99–119.

Chen, J.M., Liu, J., Leblanc, S.G., Roujean, J.-L., & Lacaze, R. (2001). Utility of multiangle remote sensing for terrestrial carbon cycle modeling. *Proceedings of the Symposium on Physical Signatures and Measurements in Remote Sensing, Aussois, France, 8–13 January* (pp. 249–260). Toulouse, France: CNES.

Chen, J. M., Pavlic, G., Brown, L., Cihlar, J., Leblanc, S. G., White, H. P., Hall, R. J., Peddle, D., King, D. J., Trofymow, J. A., Swift, E., Van der Sanden, J., & Pellikka, P. (2002). Validation of Canada-wide leaf area index maps using ground measurements and high and moderate resolution satellite imagery. *Remote Sensing of Environment*, *80*, 165–184.

Chen, J. M., Rich, P. M., Gower, S. T., Norman, J. M., & Plummer, S. (1997). Leaf area index of boreal forests: theory, techniques, and measurements. *Journal of Geophysical Research*, *102*, 29429–29443.

Cihlar, J., Chen, J. M., & Li, Z. (1997). Seasonal AVHRR multichannel data sets and products for studies of surface–atmosphere interactions. *Journal of Geophysical Research*, *102*, 29625–29640.

Diner, D. J., Asner, G. P., Davies, R., Knyazikhin, Y., Muller, J. P., Nolin, A. W., Pinty, B., Schaaf, C. B., & Stroeve, J. (1999). New directions in Earth observing: scientific application of multi-angle remote sensing. *Bulletin of the American Meteorological Society*, *80*, 2209–2228.

Du Pury, D. G. G., & Farquhar, G. D. (1997). Simple scaling of photosynthesis from leaves to canopies without the errors of big-leaf models. *Plant, Cell and Environment*, *20*, 537–557.

Farquhar, G. D., von Caemmerer, S., & Berry, J. A. (1980). A biochemical model of photosynthetic CO_2 assimilation in leaves of C_3 species. *Planta*, *149*, 78–90.

Foley, J. A. (1994). Net primary productivity in the terrestrial biosphere: the application of a global model. *Journal of Geophysical Research*, *99*, 20773–20783.

Goetz, S. J., & Prince, S. D. (1998). Variability in carbon exchange and light utilization among boreal forest stands: implications for remote sensing of net primary production. *Canadian Journal of Forest Research*, *28*, 375–389.

Goulden, M. L., Daube, B. C., Fan, S.-M., Sutton, D. J., Bazzaz, A., Munger, J. W., & Wofsy, S. C. (1997). Physiological responses of a black spruce forest to weather. *Journal of Geophysical Research*, *102*, 28987–28996.

Goward, S. N., & Huemmrich, K. E. (1992). Vegetation canopy PAR absorptance and the Normalized Difference Vegetation Index: an assessment using the SAIL model. *Remote Sensing of Environment*, *39*, 119–140.

Gower, S. T., Vogel, J. G., Norman, J. M., Kucharik, C. J., Steele, S. J., & Stow, T. K. (1977). Carbon distribution and aboveground net primary productivity in aspen, jack pine, and black spruce stands in Saskatchewan and Manitoba, Canada. *Journal of Geophysical Research*, *102*, 29029–29041.

Gu, L., Baldocchi, D. D., Verma, S. B., Black, T. A., Vesala, T., Falge, E. M., & Dowty, P. R. (2002). Superiority of diffuse radiation for terrestrial ecosystem productivity. *Journal of Geophysical Research*, *107*, 101029–101042.

Hall, F. G., Huemmrich, K. F., Goetz, S. J., Sellers, P. J., & Nickeson, J. E. (1992). Satellite remote sensing of surface energy balance: success, failures, and unresolved issue in FIFE. *Journal of Geophysical Research*, *97*, 19061–19089.

Hunt, E. R., Piper, S. C., Nemani, R., Keeling, C. D., Otto, R. D., & Running, S. W. (1996). Global net carbon exchange and intra-annual atmospheric CO_2 concentrations predicted by an ecosystem simulation model and three-dimensional atmospheric transport model. *Global Biogeochemical Cycles*, *10*, 431–456.

Jarvis, P. G., & Morison, J. I. L. (1981). Stomatal control of transpiration and photosynthesis. In P. G. Jarvis, & T. A. Mansfield (Eds.), *Stomatal physiology* (pp. 247–279). New York: Cambridge Univ. Press.

Kim, J., & Verma, S. B. (1991). Modeling canopy photosynthesis: scaling

up from a leaf to canopy in a temperate grassland ecosystem. *Agricultural and Forest Meteorology*, *57*, 187–208.

Kimball, J. S., Thornton, P. E., White, M. A., & Running, S. W. (1997). Simulating forest productivity and surface–atmosphere carbon exchange in the BOREAS study region. *Tree Physiology*, *17*, 589–599.

Knyazikhin, Y., Martonchik, J. V., Diner, D. J., Myneni, R. B., Verstraete, M. M., Pinty, B., & Gobron, N. (1998). Estimation of vegetation canopy leaf area index and fraction of absorbed photosynthetically active radiation from atmosphere corrected MISR data. *Journal of Geophysics*, *103*(D24), 32239–32256.

Kucharik, C. J., Norman, J. M., Murdock, L. M., & Gower, S. T. (1997). Characterizing canopy nonrandomness with a Multiband Vegetation Imager (MVI). *Journal of Geophysical Research*, *102*(D24), 29455–29473.

Lacaze, R., Chen, J. M., Roujean, J.-L., & Leblanc, S. G. (2002). Retrieval of vegetation clumping index using hot spot signatures measured by multiangular POLDER instrument. *Remote Sensing of Environment*, *79*, 84–95.

Lai, C.-T., Katul, G., Oren, R., Ellsworth, D., & Shafer, K. (2000). Modeling CO_2 and water vapour turbulent flux distributions within a forest canopy. *Journal of Geophysical Research*, *105*(D21), 26333–26351.

Leblanc, S. G., & Chen, J. M. (2001). A Windows Graphic User Interface (GUI) for the five-scale model for fast BRDF simulations. *Remote Sensing Reviews*, *19*, 293–305.

Leblanc, S.G., Chen, J.M., White, P.H., Cihlar, J., Roujean, J.-L., & Lacaze, R. (2001). Mapping vegetation clumping index from directional satellite measurements. *Proceedings of the Symposium on Physical Signatures and Measurements in Remote Sensing, Aussois, France, 8–13 January* (pp. 450–459). Toulouse, France: CNES.

Li, Z., & Moreau, L. (1996). A new approach for estimating photosynthetically active radiation absorbed by canopy from space: I. Total surface absorption. *Remote Sensing of Environment*, *55*, 175–191.

Liang, S., Strahler, A. H., Barnsley, M. J., Boreal, C. C., Gerstl, S. A. W., Diner, D. J., Prata, A. J., & Wlathall, C. L. (2000). Multiangle remote sensing: past, present and future. *Remote Sensing Reviews*, *18*, 83–102.

Liu, J., Chen, J. M., Cihlar, J., & Chen, W. (1999). Net primary productivity distribution in the BOREAS region from a process model using satellite and surface data. *Journal of Geophysical Research*, *104*, 27735–27754.

Liu, J., Chen, J.M., Cihlar, J., & Chen, W. (2002). Net primary productivity mapped for Canada at 1 km resolution. *Ecology and Biogeography*, *11*, 115–129.

McNaughton, K. G., & Jarvis, P. G. (1991). Effects of spatial scale on stomatal control of transpiration. *Agricultural and Forest Meteorology*, *54, 279–301.*

Monteith, J. L. (1972). Solar radiation and productivity in tropical ecosystem. *Journal of Applied Ecology*, *9*, 746–766.

Monteith, J. L. (1973). *Principles of environmental physics* (1st ed.). London: Edward Arnold.

Myneni, R. B., Nemani, R. R., & Running, E. W. (1997). Algorithm for the estimation of global land cover, LAI and FPAR based on radiative transfer models. *IEEE Transactions on Geoscience and Remote Sensing*, *35*, 1380–1393.

Nilson, T. (1971). A theoretical analysis of the frequency of gaps in plant stands. *Agricultural and Forest Meteorology*, *8*, 25–38.

Norman, J. M. (1993). Scaling processed between leaf and canopy levels. In J. R. Ehleringer, & C. B. Field (Eds.), *Scaling physiological processes: leaf to globe* (pp. 41–76). San Diego: Academic Press.

Potter, C. S., Randerson, J. T., Field, C. B., Matson, P. A., Vitousek, P. M., Mooney, H. A., & Klooster, S. A. (1993). Terrestrial ecosystem production: a process model based on global satellite and surface data. *Global Biogeochemical Cycles*, *7*, 811–841.

Prince, S. D., & Goward, S. N. (1995). Global primary production: a remote sensing approach. *Journal of Biogeography*, *22*, 815–835.

Raupack, M. R., & Finnigan, J. J. (1988). Single-layer models of evaporation from plant canopies are incorrect, but useful, whereas multiplayer models are correct but useless: discuss. *Australian Journal of Plant Physiology*, *15*, 705–716.

Ruimy, A., Dedieu, G., & Saugier, B. (1996). TURC: a dinostic model of continental grass primary productivity and net primary productivity. *Global Biogeochemical Cycles*, *10*(2), 269–285.

Running, S. W., Nemani, R. R., Peterson, D. L., Band, L. E., Potts, D. F., Pierce, L. L., & Spanner, M. A. (1989). Mapping regional forest evapotranspiration and photosynthesis by coupling satellite data with ecosystem simulation. *Ecology*, *70*, 1090–1101.

Sandmeier, S., & Deering, D. W. (1999). Structure analysis and classification of boreal forests using hyperspectral BRDF data from ASAS. *Remote Sensing of Environment*, *69*(3), 281–295.

Sellers, P. J., Berry, J. A., Collatz, G. J., Field, C. B., & Hall, F. G. (1992). Canopy reflectance, photosynthesis, and transpiration: III. A reanalysis using improved leaf models and a new canopy integration scheme. *Remote Sensing of Environment*, *42*, 187–216.

Sellers, P. J., Los, S. O., Tucker, C. J., Justice, C. O., Dazlich, D. A., Collatz, G. J., & Randall, D. A. (1996). A revised land surface parameterization (SiB2) for atmospheric GCMs: Part II. The generation of global fields of terrestrial biophysical parameters from satellite data. *Journal of Climate*, *9*, 706–737.

Shuttleworth, W. J. (1989). Micrometeorology of temperate and tropical forest. *Philosophical Transactions of the Royal Society of London*, *B324*, 299–334.

Veroustraete, P. J., & Myneni, R. B. (1996). Estimating net ecosystem exchange of carbon using the normalized difference vegetation index and an ecosystem model. *Remote Sensing of Environment*, *58*, 115–130.

Wang, Y.-P., & Leuning, R. (1998). A two-leaf model for canopy conductance, photosynthesis and partitioning of available energy: I. Model description and comparison with a multi-layered model. *Agricultural and Forest Meteorology*, *91*, 89–111.

Wofsy, S.C., Goulden, M.L., Daube, B.C., Munger, J.W., Fan, S.M., Sutton, D.J., & Bazzaz, A. (2000). Eddy correlation flux measurements of CO_2 for BOREAS. In J. Newcomer, D. Landis, S. Conrad, S. Curd, K. Huemmrich, D. Knapp, A. Morrell, J. Nickeson, A. Papagno, D. Rinker, R. Strub, T. Twine, F. Hall, & P. Sellers (Eds.), *Collected data of the boreal ecosystem–atmosphere study*. Greenbelt, USA: NASA (CD-ROM).